Inorg. Chem. **2007**, *46*, 2417–2426

Localization and Delocalization in a Mixed-Valence Dicopper Helicate

John C. Jeffery,*,† Thomas Riis-Johannessen,*,† Callum J. Anderson,† Christopher J. Adams,† Adam Robinson,† Stephen P. Argent,‡ Michael D. Ward,‡ and Craig R. Rice§

School of Chemistry, University of Bristol, Bristol BS8 1TS, U.K., Department of Chemistry, University of Sheffield, Sheffield S3 7HF, U.K., and Department of Chemical and Biological Sciences, University of Huddersfield, Huddersfield HD1 3DH, U.K.

Received August 9, 2006

The coordination chemistry of the tetradentate pyridyl-thiazole (py-tz) N-donor ligand 6,6′-bis(4-phenylthiazol-2-yl)-2,2′-bipyridine (**L^1**) has been investigated. Reaction of **L^1** with equimolar copper(II) ions results in the formation of the single-stranded mononuclear complex [Cu(**L^1**)$(ClO_4)_2$] (**1**), whereas reaction with copper(I) ions results in the double-stranded dinuclear helicate $[Cu_2(\mathbf{L^1})_2][PF_6]_2$ (**2**). Both complexes were characterized by X-ray crystallography, UV–vis spectroscopy, and electrospray ionization mass spectroscopy (as well as ^{1}H NMR spectroscopy for diamagnetic **2**). Complex **2** is redox-active and, upon one-electron oxidation, forms the stable tricationic mixed-valence helicate $[Cu_2(\mathbf{L^1})_2]^{3+}$ (**3**). This species can also be prepared in situ by combining $[Cu(MeCN)_4][BF_4]$, $[Cu(H_2O)_6][BF_4]_2$, and **L^1** in a 1:1:2 ratio in nitromethane. X-ray crystallographic analysis of **3** provides structural evidence for the presence of an internuclear Cu–Cu bond, with an even distribution of spin density across the two Cu centers. Room-temperature UV–vis spectroscopy is consistent with this finding; however, frozen-glass EPR spectroscopic investigations suggest solvatochromic behavior at 110 K, with the $[Cu_2]^{3+}$ core varying from localized to delocalized depending on the solvent polarity.

Introduction

Of the many elaborate metallosupramolecular architectures described in literature reports over the past 30 years, helicates are among those most frequently addressed.[1−4] Their ubiquitous structural motifs lend them significant aesthetic and biomimetic appeal,[1a−c,3] while from a synthetic perspective, they offer vast potential for (i) incorporating two or more metals into a polynuclear array[1] and (ii) probing the mechanistic and energetic aspects of multicomponent self-assembly processes at a fundamental level.[2]

Ever since early studies by the groups of Lehn,[3] Constable,[4] and Potts[5] established the versatile complexation properties of the *oligo*-pyridine derivatives, a wide range of polydentate ligands has been developed for the formation of helicate complexes.[1] Notable examples include the bis-catecholate O-donor ligands of Raymond et al.,[1d,6] the benzenedithiol ligands of Hahn et al.,[7] the pyrazole-phenol N,O donors of Ward et al.,[8] and the pyridyl-benzimidazole/amido mixed N,N/N,O donors of Piguet et al.[1c,2,9] By careful consideration of the donor-atom disposition and structural

* To whom correspondence should be addressed. E-mail: T.Riis-Johannessen@bristol.ac.uk.
† University of Bristol.
‡ University of Sheffield.
§ University of Huddersfield.

(1) (a) Hannon, M. J.; Childs, L. J. *Supramol. Chem.* **2004**, *16*, 7. (b) Albrecht, M. *Chem. Rev.* **2001**, *101*, 3457. (c) Piguet, C.; Bernardinelli, G.; Hopfgartner, G. *Chem. Rev.* **1997**, *97*, 2005. (d) Yeh, R. M.; Davis, A. V.; Raymond, K. N. In *Comprehensive Coordination Chemistry II*; McCleverty, J. A., Meyer, T. J., Eds.; Elsevier Ltd.: Oxford, U.K., 2004; Vol. 7, p 327.
(2) (a) Piguet, C.; Borkovec, M.; Hamacek, J.; Zeckert, K. *Coord. Chem. Rev.* **2005**, *249*, 705. (b) Hamacek, J.; Borkovec, M.; Piguet, C. *Chem. Eur. J.* **2005**, *11*, 5217. (c) Hamacek, J.; Borkovec, M.; Piguet, C. *Chem. Eur. J.* **2005**, *11*, 5227.
(3) (a) Lehn J.-M. *Supramolecular Chemistry—Concepts and Perspectives*; VCH: Weinheim, Germany, 1995. (b) Lehn, J.-M. *Angew. Chem., Int. Ed. Engl.* **1990**, *29*, 1304.
(4) Constable, E. C. In *Comprehensive Supramolecular Chemistry*; Atwood, J. L., Davies, J. E. D., Lehn, J.-M., MacNicol, D. D., Vögtle, F., Eds.; Pergamon Press: Oxford, U.K., 1996; Vol. 9, p 213.
(5) (a) Potts, K. T.; Keshavarz-K, M.; Tham, F. S.; Abruña, H. D.; Arana, C. R. *Inorg. Chem.* **1993**, *32*, 4422. (b) Potts, K. T.; Keshavarz-K, M.; Tham, F. S.; Abruña, H. D.; Arana, C. R. *Inorg. Chem.* **1993**, *32*, 4436. (c) Potts, K. T.; Keshavarz-K, M.; Tham, F. S.; Gheysen Raiford, K. A. (d) Abruña, H. D.; Arana, C. R. *Inorg. Chem.* **1993**, *32*, 4422; Potts, K. T.; Keshavarz-K, M.; Tham, F. S.; Abruña, H. D.; Arana, C. R. *Inorg. Chem.* **1993**, *32*, 4450.
(6) See, for example: (a) Yeh, R. M.; Raymond, K. N. *Inorg. Chem.* **2006**, *45*, 1130. (b) Caulder, D. L.; Raymond, K. N. *J. Chem. Soc., Dalton Trans.* **1999**, 1185. (c) Caulder, D. L.; Raymond, K. N. *Angew. Chem., Int. Ed. Engl.* **1997**, *36*, 1440.
(7) See, for example: (a) Hahn, F. E.; Isfort, C. S.; Pape, T. *Angew. Chem., Int. Ed.* **2004**, *43*, 4807. (b) Hahn, F. E.; Kreickmann, T.; Pape, T. *Dalton Trans.* **2006**, 769.

10.1021/ic061504m CCC: $37.00 © 2007 American Chemical Society
Published on Web 02/28/2007

Chart 1. Schematic Diagram of Ligands L^1-L^3

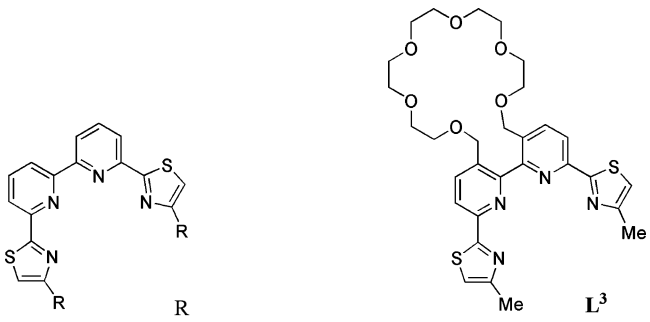

R

L¹ Ph

L² Me

L³

rigidity of the ligand backbone, many of these ligands have been designed such that adjacent donor atoms in the sequence are prevented from coordinating to a common metal ion. Accordingly, they can be considered as being *programmed* to partition into distinct binding sites, a feature that militates in favor of the formation of polynuclear helicate structures.[3]

As part of our ongoing investigations into the use of ortho-linked pyridyl-thiazole-based ligands for the assembly and control of helicate structures, we have recently been exploiting simple tetradentate N donors (**L¹**−**L³**) of the type shown in Chart 1.[10] The appeal of these ligands lies in both their synthetic accessibility[11] and their capacity to adopt one of two distinct coordination modes depending on the preference of the metal ion for a particular coordination number or geometry.[10c] The monotopic ligand **L²** behaves in a similar manner to 2,2′:6′,2″:6″,2‴-quaterpyridine (**qtpy**):[12] it forms single-stranded mononuclear complexes of the type $[M(\mathbf{L^2})]^{2+}$ with transition metal dications and double-stranded dinuclear $[M_2(\mathbf{L^2})_2]^{2+}$ complexes with the group XI monocations Cu^I and Ag^I.[10c] The behavior displayed by the ditopic crown ether derivative **L³**, however, is more remarkable.[10a,b] Binding of Ba^{2+} or Sr^{2+} ions by the μ-[18]crown-6 macrocycles in the dimercury helicate $[Hg_2(\mathbf{L^3})_2]^{4+}$, for example, causes rapid disassembly of the helicate. Within the context of ligand programming, the remote crown ether sites on **L³** thus offer the potential for the ligand to be *reprogrammed* (from double- to single-stranded coordination modes) by the sequential binding of specific s-block cations.[10a]

In this article, we report several complexes of the related ligand **L¹** with copper(I) and (II) ions and discuss their solution and solid-state structures. Our results demonstrate how the replacement of terminal methyl groups (in **L²**) with phenyl groups (in **L¹**) can dramatically alter the coordination properties of the tetradentate pyridyl-thiazole donor domains common to both ligands. In particular, self-assembly of **L¹** with Cu^I ions leads to the formation of a redox-active $[Cu_2(\mathbf{L^1})_2]^{2+}$ helicate, the (reversible) electrochemical oxidation of which is accompanied by the formation of a Cu−Cu bond and subsequent flattening of the helical pitch. Both members of the redox-related $[Cu_2(\mathbf{L^1})_2]^{2+/3+}$ pair have been structurally characterized by X-ray crystallography, and the stable tricationic $[Cu_2(\mathbf{L^1})_2]^{3+}$ helicate was further probed using UV−vis and EPR spectroscopies. The latter complex is, to the best of our knowledge, the first structurally characterized cupric helicate to exhibit a significant intermetallic bonding interaction.

Results and Discussion

Synthesis and Crystal Structure of $[Cu(L^1)(ClO_4)_2]$ (1). The copper(II) complex of **L¹** was prepared by reacting equimolar amounts of ligand with $[Cu(H_2O)_6][ClO_4]_2$ in nitromethane. Slow diffusion of diethyl ether vapor into the resulting solution afforded dark green microcrystals, for which electrospray ionization mass spectroscopy and elemental analysis suggested the formulation $[Cu(\mathbf{L^1})(ClO_4)_2]$. The solid-state structure was established by a single-crystal X-ray diffraction to be the single-stranded copper(II) complex $[Cu(\mathbf{L^1})(ClO_4)_2]\cdot MeNO_2$ (**1**·$MeNO_2$; Figure 1).

The structure of **1** closely resembles that of the previously characterized copper(II) complex of **L²** $[Cu(\mathbf{L^2})(H_2O)(ClO_4)][ClO_4]$,[10c] except that in the former, *both* axial sites on the metal are occupied by perchlorate anions, leading to a charge-neutral complex in the solid state. The respective Cu−O(1A) and Cu−O(2A) distances of 2.573(2) and 2.532(2) Å are long and reminiscent of the pseudocoordinate $Cu^{II}\cdots BF_4^-$ interactions previously reported for the tetrafluoroborate salt of bis(2,2′-bipyridine)copper(II), in which weakly bound anions occupy the remote axial sites of a Jahn−Teller distorted copper(II) system.[13]

Ligand **L¹** coordinates to the equatorial plane of the Cu^{II} center via four N donors (Figure 1), and the all-cisoid N-donor conformation brings the two terminal Ph rings into close proximity to one another at the open end of the complex. Far from causing strain at this end of the molecule, however, the interplanar distance of ca. 3.3 Å tends to suggest the presence of offset $\pi-\pi$ stacking interactions between

(8) See, for example: (a) Ronson, T. K.; Adams, H.; Riis-Johannessen, T.; Jeffery, J. C.; Ward, M. D. *New J. Chem.* **2006**, *30*, 26. (b) Ronson, T. K.; Adams, H.; Ward, M. D. *Inorg. Chim. Acta* **2005**, *358*, 1943.

(9) See, for example: (a) Zeckert, K.; Hamacek, J.; Senegas, J.-M.; Dalla-Favera, N.; Floquet, S.; Bernardinelli, G.; Piguet, C. *Angew. Chem., Int. Ed.* **2005**, *44*, 1. (b) Torelli, S.; Delahaye, S.; Hauser, A.; Bernardinelli, G.; Piguet, C. *Chem. Eur. J.* **2004**, *10*, 3503. (c) Floquet, S.; Borkovec, M.; Bernardinelli, G.; Pinto, A.; Leuthold, L.-A.; Hopfgartner, G.; Imbert, D.; Bünzli, J.-C. G.; Piguet, C. *Chem. Eur. J.* **2004**, *10*, 1091. (d) Floquet, S.; Ouali, N.; Bocquet, B.; Bernardinelli, G.; Imbert, D.; Bunzli, J.-C. G.; Hopfgartner, G.; Piguet, C. *Chem. Eur. J.* **2003**, *9*, 1860.

(10) (a) Baylies, C. J.; Harding, L. P.; Jeffery, J. C.; Riis-Johannessen, T.; Rice, C. R. *Angew. Chem., Int. Ed.* **2004**, *43*, 4515. (b) Baylies, C. J.; Riis-Johannessen, T.; Harding, L. P.; Jeffery, J. C.; Moon, R.; Rice, C. R.; Whitehead, M. *Angew. Chem., Int. Ed.* **2005**, *44*, 6909. (c) Riis-Johannessen, T.; Jeffery, J. C.; Robson, A. P. H.; Rice, C. R.; Harding, L. P. *Inorg. Chim. Acta* **2005**, *358*, 2781.

(11) (a) Rice, C. R.; Wörl, S.; Jeffery, J. C.; Paul, R. L.; Ward, M. D. *J. Chem. Soc., Dalton Trans.* **2001**, 550. (b) Rice, C. R.; Wörl, S.; Jeffery, J. C.; Paul, R. L.; Ward, M. D. *Chem. Commun.* **2000**, 1529.

(12) (a) Constable, E. C.; Elder, S. M.; Healy, J.; Tocher, D. A. *J. Chem. Soc., Dalton Trans.* **1990**, 1169. (b) Maslen, E. N.; Raston, C. L.; White, A. H. *J. Chem. Soc., Dalton Trans.* **1975**, 323. (c) Henke, Von, W.; Kremer, S.; Reinen, D. *Z. Anorg. Allg. Chem.* **1982**, *491*, 124. (d) Constable, E. C.; Elder, S. M.; Healy, J.; Ward, M. D.; Tocher, D. A. *J. Am. Chem. Soc.* **1990**, *112*, 4590. (e) Constable, E. C.; Elder, S. M.; Tocher, D. A. *Polyhedron* **1992**, *11*, 1337. (f) Constable, E. C.; Elder, S. M.; Hannon, M. J.; Martin, A.; Raithby, P. R.; Tocher, D. A. *J. Chem. Soc., Dalton Trans.* **1996**, 2423.

(13) Foley, J.; Kennefick, D.; Phelan, D.; Tyagi, S.; Hathaway, B. *J. Chem. Soc., Dalton Trans.* **1983**, 2333.

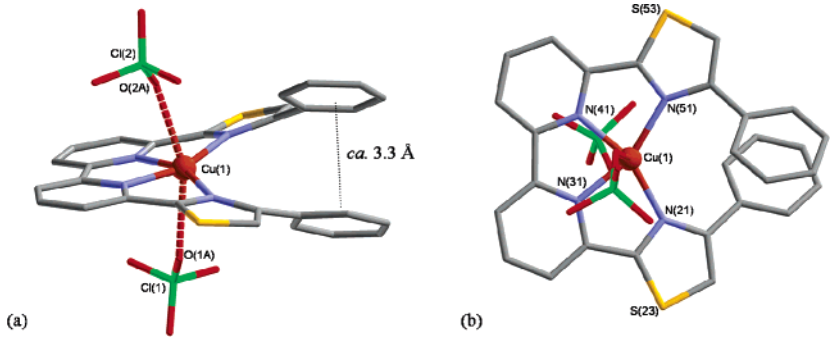

Figure 1. Two views of the solid-state structure of $[Cu(\mathbf{L^1})(ClO_4)_2]$ (**1**) with emphasis on (a) intraligand stacking interactions and (b) planar tetradentate coordination of the ligand to the Cu^{II} center.

Table 1. Selected Bond Lengths (Å) and Angles (deg) for **1**

Cu(1)−N(21)	2.027(2)	Cu(1)−N(31)	1.940(2)
Cu(1)−N(41)	1.947(2)	Cu(1)−N(51)	2.029(2)
N(31)−Cu(1)−N(41)	79.18(7)	N(31)−Cu(1)−N(21)	80.60(7)
N(41)−Cu(1)−N(21)	157.18(7)	N(31)−Cu(1)−N(51)	157.79(7)
N(41)−Cu(1)−N(51)	80.70(7)	N(21)−Cu(1)−N(51)	120.79(7)

the ligand termini (Figure 1).[14] A general pattern of long $Cu-N_{(tz)}$ and short $Cu-N_{(py)}$ bonds is apparent (Table 1), and with a Cu−N range 1.940(2)−2.029(2) Å, all metal−$\mathbf{L^1}$ bonds are significantly shorter than the equivalent bonds in $[Cu(\mathbf{L^2})(H_2O)(ClO_4)]$, for which the Cu−N separations lie in the range of 1.977(2)−2.189(2) Å.[10c]

EPR Spectroscopy. The X-band EPR spectrum of **1** in nitromethane (110 K) shows two broad features with g values of $g_{\|} = 2.28$ and $g_{\perp} = 2.08$. The low-field feature is further split into a poorly resolved quartet indicating hyperfine coupling to one Cu nucleus ($I = {}^3/_2$) with a coupling constant of $A_{\|} \approx 140$ G. These parameters are entirely typical of a copper(II) complex with approximate axial symmetry and a $(d_{x^2-y^2})^1$ ground-state configuration.[15]

Synthesis and Crystal Structure of 2. The copper(I) complex of $\mathbf{L^1}$ was similarly prepared by reacting equimolar amounts of $[Cu(MeCN)_4][PF_6]$ and ligand in nitromethane to afford a dark red solution. Diffusion of diethyl ether into the solution afforded a dark red crystalline material for which the electrospray mass spectrum (of crystals dissolved in nitromethane) showed peaks for only the dicopper(I) complex $[Cu_2(\mathbf{L^1})_2]^{2+}$. The structure was confirmed by X-ray crystallographic analysis as the dicopper(I) double-stranded helicate $[Cu_2(\mathbf{L^1})_2][PF_6]_2 \cdot MeNO_2 \cdot MeCN$ (Figure 2). Again, the structure closely resembles that of the $\mathbf{L^2}$ analogue $[Cu_2(\mathbf{L^2})_2]^{2+}$, with the two ligands being partitioned into two bis-bidentate py-tz binding domains by rotation of ca. 37.5° about the central py−py bond.[10c]

The metals are coordinated by one py-tz binding domain from each ligand, and the lack of interaction with either solvent or anion species gives the two Cu^I centers essentially identical flattened tetrahedral geometries. (The dihedral angles θ between coordinating CuNN planes are ca. 66° in each case.) With interligand separations in the range of 3.3−3.7 Å, the structure also appears to exhibit extensive $\pi-\pi$ stacking interactions between overlapping py-tz rings on adjacent ligand strands.[14]

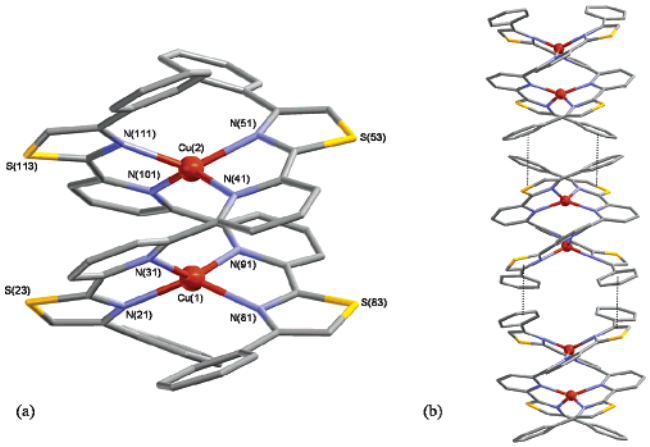

Figure 2. Solid-state structure of **2** showing (a) the (*P*)-enantiomer of the complex cation $\mathbf{2}^{2+}$ and (b) a chain of three adjacent cations $\mathbf{2}^{2+}$ (viewed along the crystallographic *b* axis) to emphasize intermolecular stacking interactions.

Table 2. Selected Bond Lengths (Å) and Angles (deg) for **2**

Cu(1)−N(21)	2.053(3)	Cu(2)−N(41)	2.058(4)
Cu(1)−N(31)	2.090(3)	Cu(2)−N(51)	2.055(3)
Cu(1)−N(81)	2.066(4)	Cu(2)−N(101)	2.055(4)
Cu(1)−N(91)	2.076(3)	Cu(2)−N(111)	2.053(4)
N(21)−Cu(1)−N(81)	134.93(13)	N(111)−Cu(2)−N(51)	134.65(14)
N(21)−Cu(1)−N(91)	117.05(13)	N(111)−Cu(2)−N(101)	81.40(14)
N(81)−Cu(1)−N(91)	80.87(15)	N(51)−Cu(2)−N(101)	111.57(14)
N(21)−Cu(1)−N(31)	80.72(12)	N(111)−Cu(2)−N(41)	114.89(13)
N(81)−Cu(1)−N(31)	110.46(13)	N(51)−Cu(2)−N(41)	81.98(15)
N(91)−Cu(1)−N(31)	142.79(13)	N(101)−Cu(2)−N(41)	142.11(14)

The feature that most distinguishes the solid-state structure of the present complex $\mathbf{2}^{2+}$ from that of previously reported $[Cu_2(\mathbf{L^2})_2]^{2+}$ is the reduction in helical pitch Δ of ca. 0.87 Å observed when the terminal methyl group is replaced by a phenyl substituent. This corresponds to a Cu···Cu separation of 2.933(1) Å in $\mathbf{2}^{2+}$ {cf. 3.805(1) Å for $[Cu_2(\mathbf{L^2})_2]^{2+}$}, and the resulting compression allows both metals to achieve a much more uniform distribution of Cu−N separations (Table 2). The change is also apparent from the decrease in py−py dihedral angle of ca. 20° on going from $[Cu_2(\mathbf{L^2})_2]^{2+}$ to $\mathbf{2}^{2+}$.[10c] Despite having a notably shorter Cu···Cu separation than both $[Cu_2(\mathbf{L^2})_2]^{2+}$ and previously reported $[Cu_2(\mathbf{qtpy})_2]^{2+}$,[12f] the value of 2.933(1) Å for $\mathbf{2}^{2+}$ is still greater than the Cu···Cu distance observed in metallic copper (2.56 Å) and lies outside the range generally accepted as constituting a

(14) Hunter, C. A.; Lawson, K. R.; Perkins, J.; Urch, C. *J. Chem. Soc., Perkin Trans. 2* **2001**, 651.
(15) Hathaway, B.; Billing, D. E. *Coord. Chem. Rev.* **1970**, *5*, 143.

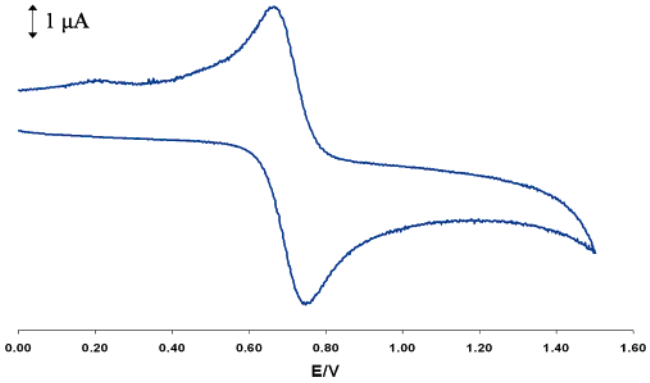

Figure 3. Cyclic voltammogram of $\mathbf{2}^{2+}$ in $MeNO_2$.

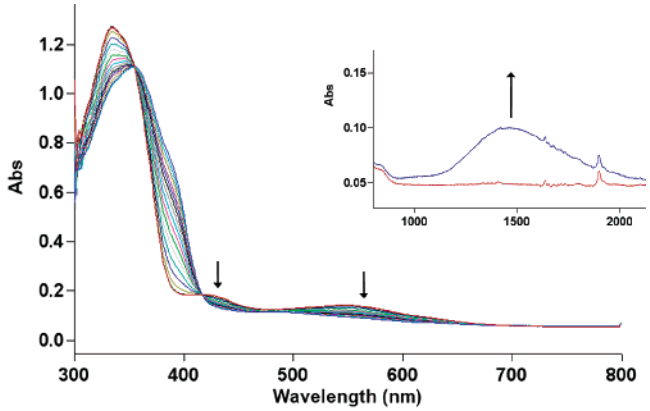

Figure 4. Evolution of the electronic (UV−vis) absorption spectrum during electrochemical oxidation of $\mathbf{2}^{2+}$ with an applied potential of +0.8 V (T = −20 °C). The inset shows the appearance of the broad transition in the near-IR region. Red and blue lines show the initial and final states, respectively.

significant bonding interaction (ca. 2.4−2.7 Å).[16] It is therefore probable that the contraction in Cu···Cu separation for **2** occurs to enable optimal overlap between the $\pi-\pi$ stacked ligand strands, although the potential influence of crystal packing interactions on solid-state geometry is also worth taking into consideration.[34]

The crystal packing arrangement of cations in the crystal structure of **2** is also of interest. Overlap between the tz and phenyl rings on adjacent molecules generates extended columns of $\pi-\pi$ stacked helicates that propagate in the crystallographic 101 direction (Figure 2b). The columns retain their screw sense throughout the entire lattice, but because it exhibits inversion symmetry, the crystal as a whole contains an equal number of both (*P*)- and (*M*)-configured helices.

^{1}H NMR Spectroscopy. The 300-MHz ^{1}H NMR spectra of $\mathbf{2}^{2+}$ in CD_3NO_2 shows a well-resolved set of seven resonances, with three pyridyl and one thiazole resonance in the range δ 7.0−7.9 and three phenyl resonances in the range δ 6.9−7.5. This is consistent with the formation of a D_2-symmetric double-stranded species, for which facile rotation of the terminal phenyl moieties renders the protons in the ortho and meta positions (relative to the tz ring) equivalent on the NMR time scale.

The chemical shifts of the py and tz resonances of $\mathbf{2}^{2+}$ appear upfield with respect to those of the single-stranded mononuclear complexes $[M(\mathbf{L^2})]^{2+}$ (where M = Zn^{II}, Cd^{II} or Hg^{II}),[10c] and all fall within the characteristic range (ca. δ 7.0−8.0) for the double-stranded helicates $[M_2(\mathbf{L^2})_2]^{2+}$ (where M = Cu^{I}, Ag^{I}).[10c] The ^{1}H NMR spectrum of $\mathbf{2}^{2+}$ is thus typical of a helicate structure in which the py-tz protons on one ligand strand are held within the shielding regions of the aromatic rings on the other strand.

Cyclic Voltammetry and UV−Vis Spectroelectrochemistry. Cyclic voltammetry of $\mathbf{2}^{2+}$ in $MeNO_2$ showed a fully reversible redox process at a potential of 0.72 V (V s SCE) (Figure 3). This behavior was maintained for scan rates ranging from 20 mV s^{-1} to 2 V s^{-1}, and the peak−peak separation ΔE_p was ca. 90 mV at a scan rate of 200 mV s^{-1}. No further redox activity was observed within the solvent-accessible potential window, and the poor solubility of the complex in other common organic solvents precluded further electrochemical characterization.

The cyclic voltammogram is consistent with fully reversible one-electron oxidation of $\mathbf{2}^{2+}$ to give a stable tricationic species for which the same overall dicopper double-stranded helicate topology is retained. This behavior contrasts with that of the $\mathbf{L^2}$ analogue $[Cu_2(\mathbf{L^2})_2]^{2+}$, which under the same conditions displayed a pseudoreversible redox process (peak−peak separation ΔE_p was ca. 200 mV at a scan rate of 200 mV s^{-1}), indicative of at least partial disassembly to give the mononuclear $[Cu^{II}(\mathbf{L^2})]^{2+}$ oxidation product.[10c]

UV−vis spectroelectrochemical investigations were carried out on a nitromethane solution containing $\mathbf{2}^{2+}$ (ca. 0.1 mM). The electronic spectrum of the dicopper(I) starting material shows two metal-to-ligand charge-transfer (MLCT) bands at ca. 420 nm (ϵ = 3500 M^{-1} cm^{-1}) and 550 nm (ϵ = 2150 M^{-1} cm^{-1}) and an additional intense band at ca. 340 nm corresponding to a ligand-based $\pi-\pi^*$ transition. The relative intensities and energies of two MLCT features—especially the relatively intense band at 550 nm—are consistent with the solution structure of $\mathbf{2}^{2+}$ retaining distorted tetrahedral copper(I) geometries ($\theta \approx 66°$) similar to those observed in the solid state.[17]

When the dicopper(I) helicate was oxidized using an applied potential of +0.8 V, successive scans showed a gradual depletion of both MLCT bands and the appearance of a shoulder at ca. 390 nm on the (red-shifted) ligand-based transition (Figure 4). Aside from the latter, the final spectrum contains only two broad bands at ca. 490 nm (ϵ = 1600 M^{-1} cm^{-1}) and 1470 nm (ϵ = 1500 M^{-1} cm^{-1}). The overlaid spectra show two isosbestic points at 360 and 420 nm, indicating clean conversion between only two species. In particular, the weak d−d transition at 650 nm (ϵ = 300 M^{-1} cm^{-1}), characteristic of the mononuclear complex **1**, is absent in the final scan, and the possibility that electrochemical oxidation causes the helicate to disassemble into mononuclear copper(II) species can thus be excluded.

(16) van Koten, G.; Noltes, J. G. In *Comprehensive Organometallic Chemistry*; Wilkinson, G., Stone, F. G. A., Abel, E., Eds.; Pergamon Press: New York, 1982; Vol. 2, Chapter 14, p 772.

(17) Ichinaga, A. K.; Kirchhoff, J. R.; McMillin, D. R.; Dietrich-Buchecker, C. O.; Marnot, P. A.; Sauvage, J.-P. *Inorg. Chem.* **1987**, *26*, 4290.

The appearance of the lowest-energy band at $\lambda = 1470$ nm (Figure 4, inset) can be attributed to one of the following: (i) a d−d transition within one $Cu^{II}N_4$ chromophore, (ii) an interaction between the two Cu centers in a localized (class II) mixed-valence dicopper system, or (iii) a transition within the d-orbital manifold of a delocalized (class III) $[Cu_2]^{3+}$ core. The first of these scenarios is very unlikely given that both its intensity ($\epsilon = 1500\ M^{-1}\ cm^{-1}$) and its wavelength (1470 nm) are significantly higher than those typically expected for d−d transitions even in tetrahedrally distorted $Cu^{II}N_4$ chromophores; these normally appear in the range of 700−1200 nm with extinction coefficients in the range $100 \leq \epsilon \leq 1000\ M^{-1}\ cm^{-1}$.[18] On this basis, the band is tentatively assigned to a transition within the $[Cu_2]^{3+}$ chromophore, although whether it corresponds to an intervalence charge-transition (IVCT) or simply an allowed transition between two orbitals encompassing both Cu ions (e.g., the HOMO → SOMO transition) is not immediately obvious. The former scenario would imply that the structure has a valence-localized Cu^{I}–Cu^{II} configuration, corresponding to a class II system in the Robin and Day classification of mixed-valence compounds, whereas the latter would imply a delocalized average-valence $Cu^{1.5}$–$Cu^{1.5}$ state, characteristic of solvent-decoupled class III behavior.[19]

A simple analysis of the bandwidth at half-height, $\Delta\bar{\nu}_{1/2}$, can provide a certain degree of insight into the nature of the transition. According to Hush theory, the relationship

$$\Delta\bar{\nu}_{1/2(calc)} \approx (2310 \times \Delta\bar{\nu}_{op})^{1/2} \approx \Delta\bar{\nu}_{1/2(obs)} \qquad (1)$$

(where $\Delta\bar{\nu}_{1/2}$ is the bandwidth at half-height and $\Delta\bar{\nu}_{op}$ is the transition energy, both in cm^{-1}) should hold for valence-localized (class II) systems, whereas in delocalized (class III) systems, $\Delta\bar{\nu}_{1/2(obs)}$ is typically much smaller than $\Delta\bar{\nu}_{1/2(calc)}$.[20] When applied to the low-energy band at 1470 nm, the observed value of $\Delta\bar{\nu}_{1/2(obs)} = 2402\ cm^{-1}$ appears significantly lower than that predicted by eq 1 ($\Delta\bar{\nu}_{1/2(calc)} \approx 3960\ cm^{-1}$), supporting the notion that the dicopper trication adopts a fully delocalized (class III) structure in solution.

In attempts to synthesize this tricationic complex directly, $[Cu(MeCN)_4][BF_4]$, $[Cu(H_2O)_6][BF_4]_2$, and $\mathbf{L^1}$ were combined in a 1:1:2 ratio in nitromethane. Diffusion of diethyl ether into the resulting solution afforded dark brown crystals, the electrospray mass spectrum of which was consistent with the expected formulation $[Cu_2(\mathbf{L^1})_2][BF_4]_3$ (**3**). The UV−vis spectrum of $[Cu_2(\mathbf{L^1})_2][BF_4]_3$ in nitromethane was found to be identical to that of the oxidized species present at the end point of the spectroelectrochemical investigations described above. Although the complex is either insoluble or unstable in most other (pure) organic solvents, no significant changes in band position or intensity were observed for spectra recorded in 1:1 nitromethane/toluene or nitromethane/dichlorobenzene mixtures. (Note that donor solvents such as MeCN, DMF, and DMSO compete with the ligand for coordination of the metal ions. This is evidenced by precipitation of the highly insoluble ligand.) Such a failure to respond to changes in solvent polarity is further diagnostic of class III or solvent-decoupled class II behavior.

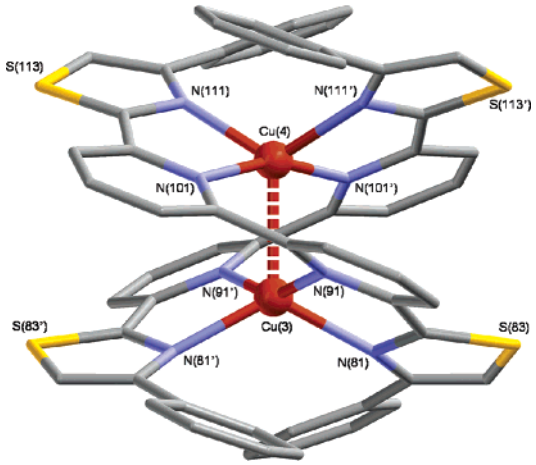

Figure 5. (*M*)-enantiomer of the complex cation (B)-$\mathbf{3}^{3+}$. The symmetry operator for generating equivalent atoms is $-x, y, 1.5 - z$.

Table 3. Selected Bond Lengths (Å) and Angles (deg) for **3**[a]

A		B	
Cu(1)−Cu(2)	2.450(1)	Cu(3)−Cu(4)	2.430(1)
Cu(1)−N(21)	2.092(2)	Cu(3)−N(81)	2.057(2)
Cu(1)−N(31)	1.969(2)	Cu(3)−N(91)	1.992(2)
Cu(2)−N(41)	1.972(2)	Cu(4)−N(101)	1.979(2)
Cu(2)−N(51)	2.058(2)	Cu(4)−N(111)	2.066(2)
N(31)−Cu(1)−N(31)	156.97(13)	N(91)−Cu(3)−N(91)	153.84(12)
N(31)−Cu(1)−N(21)	107.79(9)	N(91)−Cu(3)−N(81)	109.72(8)
N(31)−Cu(1)−N(21)	83.09(9)	N(91)−Cu(3)−N(81)	82.86(8)
N(21)−Cu(1)−N(21)	124.72(12)	N(81)−Cu(3)−N(81)	123.81(12)
N(41)−Cu(2)−N(41)	155.60(12)	N(101)−Cu(4)−N(101)	161.16(12)
N(41)−Cu(2)−N(51)	82.45(9)	N(101)−Cu(4)−N(111)	83.00(9)
N(41)−Cu(2)−N(51)	109.36(9)	N(101)−Cu(4)−N(111)	106.51(9)
N(51)−Cu(2)−N(51)	123.48(12)	N(111)−Cu(4)−N(111)	120.52(13)

[a] Symmetry operator for generating equivalent atoms: $-x, y, 1.5 - z$.

X-ray Crystallography. The solid-state structure of **3** was confirmed by X-ray crystallography as the double-stranded helicate $[Cu_2(\mathbf{L^1})_2][BF_4]_3 \cdot {}^1/_3H_2O$ ($\mathbf{3} \cdot {}^1/_3H_2O$). The structure was solved in the centrosymmetric space group $C2/c$ ($Z' = 1$), and the asymmetric unit consists of two unique $Cu(\mathbf{L^1})$ fragments, each of which grows by 2-fold rotation (about the Cu···Cu axis) to generate two crystallographically independent complex cations (A)- and (B)-$[Cu_2(\mathbf{L^1})_2]^{3+}$. One of the complex units is shown in Figure 5, and selected metric parameters for both complex units are listed in Table 3. The overall 3+ complex charge and associated mixed-/average-valence $[Cu_2(\mathbf{L^1})_2]^{3+}$ identity can be unambiguously confirmed by the presence of three noncoordinating tetrafluoroborate anions per complex cation, each of which was refined satisfactorily with full crystallographic site occupation.

The packing arrangement of $\mathbf{3}^{3+}$ trications within the lattice is similar to that observed in the crystal structure of the dicopper(I) helicate $\mathbf{2}^{2+}$. End-on overlap between the terminal tz-phenyl rings on adjacent molecules generates infinite columns of $\pi-\pi$ stacked helicates that propagate along the

(18) (a) Davis, W. D.; Zask, A.; Nakanishi, K.; Lippard, S. J. *Inorg. Chem.* **1985**, *24*, 3737. (b) Gouge, E. M.; Geldard, J. F. *Inorg. Chem.* **1978**, *17*, 270.. (c) Yokoi, H.; Addison, A. W. *Inorg. Chem.* **1977**, *16*, 1341.
(19) Robin, M. B.; Day, P. *Adv. Inorg. Chem. Radiochem.* **1967**, *10*, 247.
(20) (a) Hush, N. S. *Prog. Inorg. Chem.* **1967**, *8*, 391. (b) Creutz, C. *Prog. Inorg. Chem.* **1983**, *30*, 1.

crystallographic *b* axis. Likewise, each column contains helicates of only one screw sense, (*P*)- or (*M*)-, such that its chirality is maintained throughout the lattice. The crystal as a whole, however, is once again racemic because of the presence of inversion symmetry.

The dicopper double-stranded helicate $\mathbf{3}^{3+}$ has a structure almost identical to that of the dicopper(I) complex $\mathbf{2}^{2+}$. The ligands are similarly disposed about the central Cu−Cu axes in both complexes, conferring flattened tetrahedral geometries at the metal centers with CuNN dihedral angles θ in the range of 64−67° and Cu−N separations in the relatively narrow range of 1.969(2)−2.092(2) Å. The $Cu-N_{py}$ bonds in $\mathbf{3}^{3+}$ are marginally shorter than the remaining $Cu-N_{(tz)}$ separations (cf. $\mathbf{2}^{2+}$). The feature that most distinguishes the two complexes, however, is (again) a reduction, Δ, of ca. 0.49 Å in Cu···Cu separation on going from the dicopper dication $\mathbf{2}^{2+}$ to the trication $\mathbf{3}^{3+}$. This reduction is far greater than can be explained by simple crystal packing effects. Moreover, the corresponding Cu···Cu separations of 2.450(1) and 2.430(1) Å for the two crystallographically independent A and B cations both lie toward the short end of the range generally accepted as constituting a bonding interaction (ca. 2.4−2.7 Å).[16]

Although unprecedented in metallohelicate chemistry, comparable Cu···Cu separations have been observed in the crystal structures of a series of related $[Cu_2(L)]^{3+}$ cryptate systems (where **L** are macrotricyclic aza-cryptand ligands).[21] In the average-valence $Cu^{1.5}\cdots Cu^{1.5}$ form, complexes of this type contain two Cu ions encapsulated within the macrotricyclic host cavity, with internuclear separations in the range 2.36−2.45 Å.[21] Quantum chemical MO calculations have also been carried out in several cases, the results of which suggest that the unpaired electron occupies an orbital (SOMO) with significant σ^* antibonding Cu d_{z^2}−Cu d_{z^2} character, whereas the in-phase Cu d_{z^2}−Cu d_{z^2} combination forms the basis of a fully occupied σ bonding orbital.[21a,h] With structural evidence further supplemented by Raman, electronic, and ESR spectroscopic investigations, many of the cryptate systems were concluded to benefit from relatively strong Cu···Cu σ-bonding interactions, a feature with which the observed Cu···Cu contraction in $\mathbf{3}^{3+}$ is also clearly compatible.

The crystal structure of $\mathbf{3}^{3+}$ also provides further evidence for the high level of spin delocalization expected from the UV−vis measurements. Comparison of the Cu−N separations from each $Cu(NN)_2$ chromophore reveals minimal variation in bond length (Table 3), the mean Cu−N separations for each set of four Cu−N bonds falling in the range 2.02−2.03 Å. This implies that each pair of Cu centers has an approximately equal share of the electron spin density, as a more asymmetric distribution would give rise to two $Cu(NN)_2$ chromophores (e.g., one $Cu^{I}N_4$ and one $Cu^{II}N_4$ set) with nonequivalent geometries reflecting the different charge densities at the two metal centers. However, these observations do not account for the potential effects of dynamic or static disorder within the crystal structure [i.e., a time- or space-averaged representation of two extreme $Cu^{I}(NN)_2$ and $Cu^{II}(NN)_2$ states could make all copper centers appear identical], and concrete conclusions can be drawn only once these possibilities have been ruled out. A brief analysis of the atomic displacement parameters of each $Cu(NN)_2$ chromophore is therefore necessary in order to determine whether the ligand atoms show more displacement along the M−**L**[1] bonds than do the metal atoms to which they are attached, a likely scenario if the N-donor atoms alternate between two different positions in the crystal.[22] Although visual inspection of the anisotropic displacement parameters can provide some useful information regarding this disorder, a more rigorous approach considers the mean-square displacement amplitudes (MSDAs). These are parameters that more accurately describe the displacement of a given atom in a specified crystallographic direction, e.g., along a metal−ligand bond.[22]

Table 4. Calculated $\langle d^2 \rangle$ ($\times 10^{-4}$ Å^2) Values for All Cu−N Bonds in the Two Independent Complex Cations (A)- and (B)-$\mathbf{3}^{3+}$ [a]

A		B	
Cu(1)−N(21)	−6	Cu(1)−N(81)	−34
Cu(1)−N(31)	−4	Cu(1)−N(91)	29
Cu(2)−N(41)	7	Cu(2)−N(101)	12
Cu(2)−N(51)	7	Cu(2)−N(111)	−18

[a] Negative $\langle d^2 \rangle$ values arise when the displacement of the Cu atom along a Cu−N bond is greater than that of the coordinating N-donor atom.

$$\mathrm{MSDA} = \frac{\sum_{i=1}^{3}\sum_{j=1}^{3} U_{ij} n_i n_j}{|n|^2} \qquad (2)$$

$$\Delta\mathrm{MSDA} = \mathrm{MSDA}_{(\mathrm{ligand})} - \mathrm{MSDA}_{(\mathrm{metal})} = \langle d^2 \rangle \qquad (3)$$

The MSDAs for the Cu and N atoms in each $Cu(NN)_2$ chromophore are obtained from eq 2, where U_{ij} is the *ij*th element of the 3 × 3 tensor of anisotropic displacement parameters (Å^2) and n_i and n_j are elements of the vector $|n|$ describing the relevant Cu−N bond.[23] The $\langle d^2 \rangle$ values for the various Cu−N bonds can then be computed from eq 3 to give an indication of the extent to which the atoms of each Cu−N pair are disordered along the bond mutually connecting them. For ordered systems, the M−N bonds generally exhibit values of $\langle d^2 \rangle \ll 0.01$ Å,^{2} whereas for dynamically or statically disordered systems, $\langle d^2 \rangle \geq 0.01$ Å^2.[24] As is apparent from Table 4, the $\langle d^2 \rangle$ values obtained

(21) (a) Barr, M. E.; Smith, P. H.; Antholine, W. E.; Spencer, B. *J. Chem. Soc., Chem. Commun.* **1993**, 1649. (b) Harding, C.; McKee, V.; Nelson, J. *J. Am. Chem. Soc.* **1991**, *113*, 9684. (c) Franzen, S.; Miskowski, V. M.; Shreve, A. P.; Wallace-Williams, S. E.; Woodruff, W. H.; Ondrias, M. R.; Barr, M. E.; Moore, L.; Boxer, S. G. *Inorg. Chem.* **2001**, *40*, 6375. (d) Al-Obaidi, A.; Baranovi_c, G.; Coyle, J.; Coates, C. G.; McGarvey, J. J.; McKee, V.; Nelson, J. *Inorg. Chem.* **1998**, *37*, 3567. (e) LeCloux, D. D.; Davydov, R.; Lippard, S. J. *Inorg. Chem.* **1998**, *37*, 6814. (f) Harding, C.; Nelson, J.; Symons, M. C. R.; Wyatt, J. *J. Chem. Soc., Chem. Commun.* **1994**, 2499. (g) Farrar, J. A.; McKee, V.; Al-Obaidi, A. H. R.; McGarvey, J. J.; Nelson, J.; Thomson, A. J. *Inorg. Chem.* **1995**, *37*, 3567. (h) Farrar, J. A.; Grinter, R.; Neese, F.; Nelson, J.; Thomson, A. J. *J. Chem. Soc., Dalton Trans.* **1997**, 4083.

(22) Falvello, L. R. *J. Chem. Soc., Dalton Trans.* **1997**, 4463.

(23) Dunitz, J. D.; Schomaker, V.; Trueblood, K. N. *J. Chem. Phys.* **1988**, *92*, 856.

(24) Hathaway, B. J. *Struct. Bonding (Berlin)* **1984**, *57*, 55.

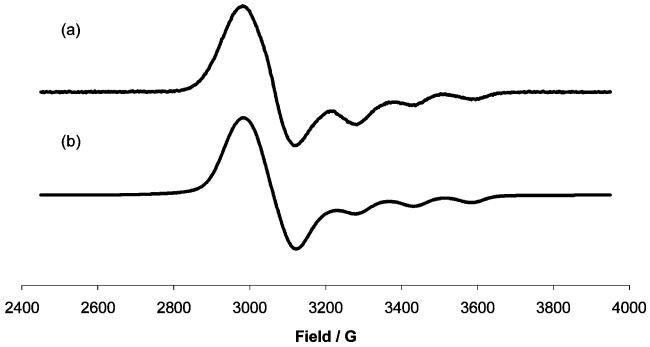

Figure 6. X-band EPR spectrum of $\mathbf{3}^{3+}$ in $MeNO_2$ at 110 K: (a) experiment and (b) simulation.

for both (A)- and (B)-$\mathbf{3}^{3+}$ all fall well within the range expected for ordered systems, and it can therefore be concluded that the uniform distribution of Cu−N bond lengths reflects a genuinely high level of spin delocalization in the solid-state complex.

EPR Spectroscopy. The EPR spectra of compounds displaying mixed- or average-valence behavior can yield a wealth of information regarding electronic structure and spin distribution over a wide range of conditions. For dicopper systems with one fully delocalized unpaired electron, hyperfine coupling of the electron to two equivalent Cu ($I = {}^3/_2$) nuclei often gives a characteristic seven-line spectrum. In contrast, in valence-localized states, the electron interacts with only one nucleus on the EPR time scale, and hyperfine coupling to *one* Cu ($I = {}^3/_2$) nucleus results in a four-line spectrum. Although this is the general case, it should be noted that EPR observation of mixed- or average-valence behavior can be extremely sensitive to the experimental conditions and several systems have been reported in which the degree of spin delocalization is strongly dependent on temperature. This effect normally takes the intuitive form: on reaching sufficiently low temperatures, a delocalized (ambient-temperature) system gets *trapped in a valence-localized state*.[25] However, the converse was also observed by Ward et al., who reported the first mixed-valence tricopper complex in which spin delocalization occurred only below 120 K, the valence-localized form becoming more abundant at higher temperatures.[26]

The X-band EPR spectra of $\mathbf{3}^{3+}$ in pure nitromethane ($MeNO_2$), 1:1 nitromethane/toluene ($MeNO_2$/tol), and 1:1 nitromethane/dichlorobenzene ($MeNO_2$/DCB) mixtures were recorded at 110 K. The frozen-glass spectra of $\mathbf{3}^{3+}$ in pure $MeNO_2$ and a 1:1 $MeNO_2$/DCB mixture are essentially identical and fully consistent with a spin-localized structure (Figure 6). In both cases, $g_x = 2.25$, $g_y = 2.18$, and $g_z = 2.01$, giving a $g_x \geq g_y > g_z > 2.00$ pattern characteristic of a copper(II) complex with approximate axial symmetry and a $(d_{z2})^1$ ground-state configuration.[15] The feature at low field is further split into a well-resolved quartet, indicating hyperfine coupling to *one* Cu nucleus ($I = {}^3/_2$) with a coupling constant of $A_z \approx 150$ G.

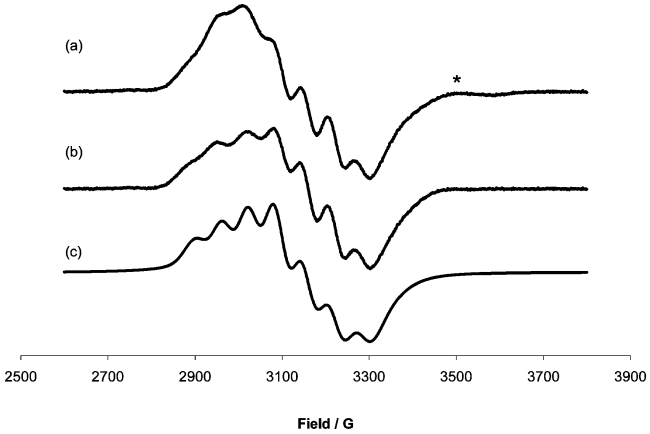

Figure 7. (a) Frozen-glass X-band EPR spectrum of $\mathbf{3}^{3+}$ recorded in a 1:1 $MeNO_2$/toluene mixture (110 K). The asterisk * highlights the weak inflection at ca. 3580 G. (b) Spectrum a corrected by subtraction of a small amount of the spectrum obtained in $MeNO_2$ (Figure 6a). (c) Simulation of spectrum b based on hyperfine coupling to two identical Cu ($I = {}^3/_2$) nuclei ($g_\perp = 2.17$, $g_\parallel = 2.08$, and $A_\perp \approx 62$ G).

The spectrum of $\mathbf{3}^{3+}$ in a 1:1 nitromethane/toluene mixture is somewhat different from the above, and a total of seven lines can just about be discerned on the main feature, in addition to a weak inflection that appears at ca. 3580 G (Figure 7a). The spectrum could be interpreted as representative of a fully spin-delocalized system, with $g_\perp = 2.17$ and $g_\parallel = 2.08$ and hyperfine coupling of the unpaired electron to *two* equivalent Cu ($I = {}^3/_2$) nuclei on the low-field component ($A_\perp \approx 62$ G) to give the expected septet. ($A_\parallel$ was not included in this simulation.) However, equally satisfactory simulations were obtained using a valence-localized model, which involves coupling to one Cu ($I = {}^3/_2$) nucleus, with $g_x = 2.25$, $g_y = 2.15$, and $g_z = 2.04$ and hyperfine coupling constants for the two low-field components of $A_x = 45$ and $A_y = 60$ G. In this interpretation, although the electron is coupled to only one nucleus, the hyperfine splitting observed on both the (sufficiently well resolved) g_x and g_y components gives rise to two overlapping quartets that, in turn, resemble a poorly resolved septet.

It is worth noting that neither of the two models described above accounts for the weak inflection observed at ca. 3580 G. Given its proximity to the highest-field feature in the four-line spectra obtained for pure $MeNO_2$ and $MeNO_2$/DCB glasses (Figure 6), this feature could be due to trace amounts of the (apparently) valence-localized species observed in the latter. Indeed, the inflection is effectively *removed* by subtracting a small amount (ca. 10%) of the $MeNO_2$ spectrum (Figure 6) from that recorded in the $MeNO_2$/tol glass (Figure 7a) to give the corrected spectrum shown in Figure 7b. This also improves somewhat the resolution of the low-field feature and likewise its resemblance to the simulation based on coupling to two equivalent Cu ($I = {}^3/_2$) nuclei (Figure 7c).

The degree of spin delocalization in $[Cu_2(\mathbf{L}^1)_2]^{3+}$ thus appears highly susceptible to variations in both phase and conditions. UV−vis spectra and X-ray crystallographic data suggest class III behavior for the (ambient-temperature)

(25) See, for example: (a) Gagné, R. R.; Koval, C. A.; Smith, T. J.; Cimolino, M. C. *J. Am. Chem. Soc.* **1979**, *101*, 4571. (b) Long, R. C.; Hendrickson, D. N. *J. Am. Chem. Soc.* **1983**, *105*, 1513.

(26) Jones, P. L.; Jeffery, J. C.; Maher, J. P.; McCleverty, J. A.; Rieger, P. H.; Ward, M. D. *Inorg. Chem.* **1997**, *36*, 3088.

solution-phase, and (low-temperature, 100 K) solid-state forms, but in the frozen glass (110 K), EPR measurements begin to expose solvatochromic tendencies. Spin delocalization is observed when the spectrum is recorded in a 1:1 $MeNO_2$/tol glass, whereas spectra recorded in pure $MeNO_2$ or 1:1 $MeNO_2$/DCB glasses show only a spin-localized species.

An attractive explanation for this behavior requires consideration of the overall solvent polarity in each system. Exchanging pure $MeNO_2$ for a $MeNO_2$/tol mixture effectively constitutes a significant reduction in polarity of the medium surrounding each trication in both the solution and frozen glass. Clearly, at room temperature, this change in polarity has a negligible influence on the spin distribution. At 110 K, however, the combination of low temperature and a highly polar $MeNO_2$ glass (the dielectric constants for $MeNO_2$, DCB, and toluene are 39.4, 2.8, and 1.0, respectively) results in the trapping of a valence-localized state (on the EPR time scale). On introducing toluene, a system crossover from spin-localized to spin-delocalized begins to occur as the glass is no longer sufficiently polar to fully stabilize the large dipole moment associated with a valence-localized state. That the resolution of the (delocalized) seven-line spectrum can be improved by removing a ca. 10% contribution from the (valence-localized) four-line spectrum is, however, also consistent with the retention of a small quantity of the valence-localized form.

Conclusion

The mononuclear copper(II) complex $[Cu(L^1)(ClO_4)_2]$ (**1**) and the dinuclear helicate redox-related pair $[Cu_2(\mathbf{L^1})_2]^{2+/3+}$ ($\mathbf{2}^{2+}$ and $\mathbf{3}^{3+}$, respectively) have been isolated and characterized using a combination of X-ray crystallography; cyclic voltammetry; and ESI-MS, UV−vis, ^{1}H NMR, and EPR spectroscopies. The solid-state structures of **1** and $\mathbf{2}^{2+}$ closely resemble those of their previously reported (methyl-substituted) $\mathbf{L^2}$ analogues.[10c] The impact of replacing the terminal Me groups in $\mathbf{L^2}$ for phenyl groups in $\mathbf{L^1}$ is instead manifested in the electrochemical behavior of $\mathbf{2}^{2+}$. Whereas oxidation of $[Cu_2(\mathbf{L^2})_2]^{2+}$ is pseudoreversible and causes partial disassembly of the helicate structure, $\mathbf{2}^{2+}$ readily loses one electron to form a stable tricationic helicate $[Cu_2(\mathbf{L^1})_2]^{3+}$ ($\mathbf{3}^{3+}$). The latter displays an average-valence electronic structure under ambient conditions and can be synthesized in situ by combining a 1:1:2 ratio of $[Cu(MeCN)_4][BF_4]$, $[Cu(H_2O)_6][BF_4]_2$, and $\mathbf{L^1}$ in nitromethane. X-ray crystallographic analysis of the resulting compound also provides evidence of a Cu−Cu bonding interaction.

We suggest that the formation and apparent stability of average-valence $\mathbf{3}^{3+}$ can be attributed to the $\pi-\pi$ stacking ability of the terminal phenyl substituents on $\mathbf{L^1}$. With Me groups in the same positions in $\mathbf{L^2}$, the $[Cu_2(\mathbf{L^2})_2]^{2+}$ helicate is constrained to adopt conformations in which steric congestion between the Me groups on one ligand and the py rings on the other is reduced. This is liable to prevent the helical pitch of $[Cu_2(\mathbf{L^2})_2]^{2+}$ from contracting sufficiently to allow Cu−Cu bond formation. In contrast, the heightened potential for extensive $\pi-\pi$ overlap to occur between adjacent strands of (phenyl-substituted) $\mathbf{L^1}$ imparts the necessary flexibility on $\mathbf{2}^{2+}$ to accommodate structural contraction. Indeed, given the ease with which $\mathbf{3}^{3+}$ undergoes self-assembly in situ, it is not unreasonable to assume that the interligand stacking and Cu−Cu bonding interactions in $\mathbf{3}^{3+}$ are of a complementary nature.

Experimental Section

Characterization and Physical Measurements. Electron impact (EI) mass spectra were recorded on a VG Autospec instrument. Electrospray ionization mass spectra were recorded on either a continual-flow VG Quattro II triple quadrupole mass spectrometer (with Z-spray source and cone voltages in the range of 25−40 V) or a Bruker-Daltronics Apex 4e 7.0T (FT-MS) instrument; analytes were dissolved in acetonitrile or nitromethane at concentrations of ca. 0.1 mg mL^{-1}. UV−vis spectra were recorded using a Perkin-Elmer Lambda 19 UV−vis spectrometer. Solutions were analyzed in the 0.1−1.0 mmol concentration range in quartz cells of path length 10 or 1 mm. One-dimensional ^{1}H NMR spectra were recorded on Jeol GX400 and Jeol GX270 spectrometers. EPR spectra were recorded on a Bruker ESP300E spectrometer. Measurements were made at 110 K in frozen nitromethane, 1:1 nitromethane/toluene, and 1:1 nitromethane/dichlorobenzene glasses. Data analysis and spectral simulations were performed using WINEPR and SimFonia software, respectively.[27] Electrochemical measurements were performed using an EG&G model 273A potentiostat linked to a computer with EG&G model 273 research electrochemistry software, in conjunction with a three-electrode cell. The auxiliary electrode was a platinum wire, and the working electrode was a platinum disc (1.6-mm diameter). The reference electrode was an aqueous saturated calomel electrode separated from the solution by a fine-porosity frit and an agar bridge saturated with KCl. Compounds were analyzed in 1 mM concentrations with $[N^nBu_4][PF_6]$ (0.1 M) as the supporting electrolyte. Ferrocene ($E°$ = 0.47 V) or diacetylferrocene ($E°$ = 0.97 V) was added at the end of each experiment as an internal standard. Unless otherwise stated, $(E_p)_{ox}$ and $(E_p)_{red}$ values are quoted at a scan rate of 200 mV s^{-1}. UV−vis/NIR spectroelectrochemical measurements were carried out using a Cary Varian 5000 spectrophotometer in conjunction with an optically transparent thin-layer electrode (OTTLE) cell fitted with platinum gauze, platinum wire, and Ag/AgCl working, counter, and reference electrodes, respectively. The temperature was maintained at −20 °C throughout data collection. Potentials were applied using an EG&G model 273A potentiostat linked to a computer with EG&G model 273 research electrochemistry software. UV−vis/NIR spectra were recorded every 3−5 min until electrolysis was complete. Magnetic measurements were carried out using a 5T Quantum Design SQUID magnetometer. The temperature was varied from 2 to 300 K at a rate of 2 K/min under an applied field of 1 T.

X-ray Crystallography. Crystals were visually inspected for defects and singularity under a binocular microscope fitted with a polarizing attachment. Suitable crystals were then coated with epoxy resin, mounted on a glass fiber, and quickly transferred to a Bruker-AXS PROTEUM (CCD area detector) diffractometer under a stream of cold N_2 gas. Preliminary scans were employed to assess crystal quality, lattice symmetry, ideal exposure time, etc., prior to collection of a sphere or hemisphere (for low- and high-symmetry crystal systems, respectively) of diffraction intensity data using

(27) (a) *Bruker WINEPR System*, version 2.11; Bruker-Franzen Analytik GmbH, 1990−1996. (b) *WINEPR SimFonia*, version 1.25; Bruker Analytische Messtechnik GmbH, 1994−1996.

Table 5. Crystal Data and Refinement Parameters for **1**−**3**

	1·$MeNO_2$	**2**·$MeNO_2$·MeCN	**3**·$^1/_3H_2O$
empirical formula	$C_{29}H_{21}Cl_2CuN_5O_{10}S_2$	$C_{59}H_{42}Cu_2F_{12}N_{10}O_2P_2S_4$	$C_{56}H_{36.66}B_3Cu_2F_{12}N_8O_{0.3}S_4$
formula weight	798.07	1468.29	1341.31
temperature	100(2) K	100(2) K	100(2) K
wavelength	1.54178 Å	1.54178 Å	1.54178 Å
crystal system	monoclinic	monoclinic	monoclinic
space group	$P2_1/n$	$P2/c$	$C2/c$
unit cell dimensions	$a = 15.8162(2)$ Å $b = 12.9136(2)$ Å $c = 16.8236(2)$ Å $\alpha = 90°$ $\beta = 114.0750(10)°$ $\gamma = 90°$	$a = 18.7741(8)$ Å $b = 19.6516(8)$ Å $c = 17.3283(8)$ Å $\alpha = 90°$ $\beta = 115.311(2)°$ $\gamma = 90°$	$a = 27.2491(6)$ Å $b = 18.7615(5)$ Å $c = 24.5663(6)$ Å $\alpha = 90°$ $\beta = 121.9390(10)°$ $\gamma = 90°$
volume	3137.22(7) Å^3	5779.4(4) Å^3	10657.8(5) Å^3
Z (Z)	4 (1)	4 (1)	8 (1)
density (calcd)	1.690 Mg/m^3	1.687 Mg/m^3	1.672 Mg/m^3
absorption coefficient	4.388 mm^{-1}	3.615 mm^{-1}	3.261 mm^{-1}
F(000)	1620	2968	5405
crystal size	0.3 × 0.2 × 0.1 mm	0.2 × 0.05 × 0.02 mm	0.3 × 0.2 × 0.1 mm
θ range	3.23−70.04°	2.25−70.22°	3.03−70.16°
index ranges	$-19 \le h \le 18$, $-15 \le k \le 15$, $-17 \le l \le 19$	$-22 \le h \le 22$, $-23 \le k \le 23$, $-21 \le l \le 21$	$-33 \le h \le 33$, $-22 \le k \le 22$, $-22 \le l \le 29$
reflections collected	14802	42831	29837
independent reflections	5147 ($R_{int} = 0.0316$)	10738 ($R_{int} = 0.0723$)	8828 ($R_{int} = 0.0296$)
data/restraints/parameters	5147/0/526	10738/0/763	8828/0/777
GOF on F^2	$S = 1.034$	$S = 1.046$	$S = 1.046$
R indices [$I > 2\sigma(I)$][a−c]	R1 = 0.0315, wR2 = 0.0826	R1 = 0.0567, wR2 = 0.1304	R1 = 0.0404, wR2 = 0.1121
R indices (all data)[a,b,d]	R1 = 0.0355, wR2 = 0.0853	R1 = 0.0985, wR2 = 0.1455	R1 = 0.0444, wR2 = 0.1155
weighting scheme[b]	$a = 0.0525$, $b = 1.1740$	$a = 0.0676$, $b = 0.7040$	$a = 0.0671$, $b = 18.3342$
largest diff peak and hole	0.349 and −0.552 eÅ^{-3}	0.592 and −0.746 eÅ^{-3}	1.033 and −0.658 eÅ^{-3}

[a] Structure was refined on F_o^2 using all data; the value of R1 is given for comparison with older refinements based on F_o with a typical threshold of $F \ge 4\sigma(F)$. [b] wR2 = $[\sum[w(F_o^2 - F_c^2)^2]/\sum w(F_o^2)^2]^{1/2}$, where $w^{-1} = [\sigma^2(F_o^2) + (aP)^2 + bP]$ and $P = [\max(F_o^2,0) + 2F_c^2]/3$. [c] 4577 reflections with $I > 2\sigma(I)$. [d] All 5147 data.

SMART operating software.[28] Intensities were then integrated from several series of exposures (each exposure covering 0.3° in ω), merged, and corrected for Lorentz and polarization effects using SAINT software.[29] Solutions were generated by conventional heavy-atom Patterson or direct methods and refined by full-matrix nonlinear least-squares on all F^2 data, using SHELXS-97 and SHELXL software, respectively (as implemented in the SHELXTL suite of programs).[30] Empirical absorption corrections were applied based on multiple and symmetry-equivalent measurements using SADABS,[31] and where stated, the scattering contributions from diffuse solvent moieties were removed using the SQUEEZE function in PLATON.[32] All structures were refined until convergence (max shift/esd <0.01), and in each case, the final Fourier difference map showed no chemically sensible features. Crystallographic refinement parameters are summarized in Table 5.

Synthesis of 6,6′-Bis(4-phenylthiazol-2-yl)-2,2′-bipyridine (L^1). An excess of chloroacetophenone was added to a two-necked round-bottom flask, fitted with a condenser, containing a suspension of 6,6′-bis(thiocarboxyamide)-2,2′-bipyridine[33] (0.873 g, 3.16 mmol) in ethanol (50 mL). The mixture was brought to reflux and stirred for 4 h, during which two more portions of chloroacetophenone were added. The reaction mixture was left at reflux for an additional 4 h, resulting in total loss of the initial yellow color. Cooling followed by concentration under reduced pressure gave an off-white precipitate that was collected by filtration and suspended in aqueous ammonia solution overnight. The solid was then filtered and washed in cold ethanol to give 6,6′-bis(4-phenylthiazol-2-yl)-2,2′-bipyridine (**L^1**) as a tan powder (yield: 80%). Found C, 70.65; H, 3.59; N, 11.11%. $C_{28}N_4S_2H_{18}$ requires C, 70.86; H, 3.82; N, 11.81%. High-resolution EI-MS m/z 474.096153 ([M]$^+$) (calcd for $C_{28}H_{18}N_4S_2$, 474.097290; deviation, 2.4 ppm). The poor solubility of **L^1** in common organic solvents precluded characterization by NMR spectroscopy.

Metal Complexes. The complexes were prepared by combining equimolar amounts (0.029 mmol) of **L^1** with an appropriate metal salt in the minimum amount (5−10 mL) of solvent (nitromethane or acetonitrile). For $[Cu_2(\mathbf{L^1})_2][BF_4]_3$, a 1:1:2 ratio of $[Cu(H_2O)_6][BF_4]_2$, $[Cu(MeCN)_4][BF_4]$, and ligand was used. The suspensions were then gently heated, sonicated for ca. 10 min, filtered, and concentrated in vacuo (if necessary). Slow diffusion of diethyl ether into the resulting solutions afforded crystals suitable for X-ray structural analysis. ***Caution:*** *Perchlorate salts are potentially explosive and should be handled with due care.* Those complexes described below that were isolated as perchlorates were prepared in only small quantities (10−20 mg), and we did not encounter any problems with them.

Data for $[Cu(\mathbf{L^1})(ClO_4)_2]$·$MeNO_2$ (**1**): Found C, 43.63; H, 3.10; N, 8.68%. $CuC_{28}H_{18}N_4S_2O_8Cl_2$·$MeNO_2$ requires C, 43.64; H, 2.65; N, 8.78%. ESI-MS m/z 268.5 {$[Cu(\mathbf{L^1})]^{2+}$}, 505.5 {$[Cu(\mathbf{L^1})_2]^{2+}$}, 635.9 {$[Cu(\mathbf{L^1})(ClO_4)]^+$}. High-resolution ESI-MS m/z 635.9756400 {$[Cu(\mathbf{L^1})(ClO_4)]^+$} (calcd for $CuC_{28}H_{18}N_4S_2ClO_4$, 635.9748517; deviation, 1.2 ppm).

(28) *SMART Diffractometer Control Software*; Bruker Analytical X-ray Instruments Inc.: Madison, WI, 1998.

(29) *SAINT Integration Software*; Siemens Analytical X-ray Instruments Inc.: Madison, WI, 1994.

(30) *SHELXTL Program System*, version 5.1; Bruker Analytical X-ray Instruments Inc.: Madison, WI, 1998.

(31) Sheldrick, G. M. *SADABS*: *A Program for Absorption Correction with the Siemens SMART System*; University of G**öttingen: Göttingen, Germany, 1996.**

(32) Spek, A. L. ***Acta. Crystallogr.* 1990**, *A46*, C-34. *PLATON—A Multipurpose Crystallographic Tool*; Utrecht University: Utrecht, The Netherlands, 2003.

(33) For synthesis, see: Baxter, P. N. W.; Connor, J. A.; Schweizer, W. B.; Wallis, J. D. *J. Chem. Soc., Dalton Trans.* **1992**, 3015.

(34) We note that an almost identical Cu···Cu separation of 2.92 Å was observed by Thummel et al. in the dicopper(I) helicate of a tetradentate bis-1,10-phenanthroline ligand. See: Riesgo, E. C.; Hu, Y.-Z.; Thummel, R. P. *Inorg. Chem.* **2003**, *42*, 6648.

Data for $[Cu_2(\mathbf{L^1})_2][PF_6]_2 \cdot MeNO_2 \cdot MeCN$ (**2**): ESI-MS *m*/*z* 538.0 $\{[Cu_2(\mathbf{L^1})_2]^{2+}\}$, 1221.0 $\{[Cu_2(\mathbf{L^1})_2(PF_6)]^{+}\}$. High-resolution ESI-MS *m*/*z* 1363.9905520 $\{[Cu_2(\mathbf{L^1})_2(PF_6)_2]^{+}\}$ (calcd for $Cu_2C_{56}H_{36}N_8S_4P_2F_{12}$, 1363.9815910; deviation, 6.5 ppm). ^{1}H NMR (300 MHz, CD_3CN) δ 7.91 (4H, t, $J = 7.8$, pyridyl H^4), 7.88 (4H, dd, $J = 7.8$, 2.4 pyridyl H^3), 7.80 (4H, s, thiazole H^5), 7.45 (8H, d, $J = 7.8$, *ortho*-phenyl), 7.06 (4H, t, $J = 7.8$, *para*-phenyl), 7.00 (4H, dd, $J = 6.3$, 2.4, pyridyl H^5), 6.94 (8H, d, $J = 7.8$, *meta*-phenyl).

Data for $[Cu_2(\mathbf{L^1})_2][BF_4]_3 \cdot {}^1/_3H_2O$ (**3**): ESI-MS *m*/*z* 358.6 $\{[Cu_2(\mathbf{L^1})_2]^{3+}\}$, 505.5 $\{[Cu(\mathbf{L^1})_2]^{2+}\}$, 538.0 $\{[Cu_2(\mathbf{L^1})_2]^{2+}\}$, 582.0 $\{[Cu_2(\mathbf{L^1})_2(BF_4)]^{2+}\}$, 1163.1 $\{[Cu_2(\mathbf{L^1})_2(BF_4)]^{+}\}$, 1250.1 $\{[Cu_2(\mathbf{L^1})_2(BF_4)_2]^{+}\}$. High-resolution ESI-MS *m*/*z* 358.0177470 $\{[Cu_2(\mathbf{L^1})_2]^{3+}\}$ (calcd for $Cu_2C_{56}H_{36}N_8S_4$, 358.0173775; deviation, 1.0 ppm). Crystalline samples of **3** displayed typical Curie-type paramagnetic behavior, with a linear dependence of $1/M$ on T (or of M on $1/T$) according to the Curie law $M/H = C/T$.

Acknowledgment. We thank the EPSRC and the University of Bristol for financial support and the School of Chemistry (University of Bristol) Mass Spectroscopy service for obtaining mass spectra of all compounds reported herein. We also thank the EPSRC National EPR service for conducting preliminary EPR measurements.

Supporting Information Available: Crystallographic data for **1**−**3** (atomic coordinates, anisotropic displacement parameters, refinement details, etc.) in cif format and a thermal ellipsoid plot of the mixed-valence compound **3**. This material is available free of charge via the Internet at: http://pubs.acs.org.

IC061504M